

Effect of Graphene on Micro-Structure and Properties of MAO Coating Prepared on Mg-Li Alloy

Fei Chen^{}, Yulin Zhang and You Zhang*

Beijing Key Lab of Special Elastomeric Composite Materials, College of Materials Science and Engineering, Beijing Institute of Petrochemical Technology, Beijing 102617, China

*E-mail: chenfei_bipt@126.com

Received: 24 March 2017 / Accepted: 29 April 2017 / Published: 12 June 2017

Ceramic coating modified with graphene was formed on Mg-Li alloy by a micro-arc oxidation process in a graphene powders (GE) added silicate electrolyte. The microstructure, composition, tribological and corrosion behaviors of the coatings were performed. The results showed that the added GE promote the formation of hard MgO and SiO₂ phases in MAO film and result in low friction coefficient and enhanced wear resistance. C element was also detected on the surface of the GE added film. With the addition of GE in silicate electrolyte, the corrosion resistance of the composite coating was improved significantly owing to the pore size decreases and film thickness increases.

Keywords: Micro-arc oxidation; Graphene; Wear resistance; Corrosion resistance

1. INTRODUCTION

Magnesium and its alloys are the lightest structure metal because of their high strength-to-weight, good dimensional stability, casting potentials, and weld-ability[1-2]. However the comparatively poor wear and corrosion resistance of magnesium alloys have restricted the widespread application in automotive industries[3-4]. In answer to this, multiple studies have been carried out to improve the surface performance of light metals[5-6]. Several reports have revealed that surface treatment methods such as electro-deposition, Physical Vapour Deposition, plasma spraying, ion implantation, etc. are used to improve the surface properties of Mg alloys[7-8]. In addition, Micro-arc oxidation (MAO) as an promising surface engineering technology has been widely used to fabricate coatings with admirable properties: high hardness, good corrosion resistance and excellent bonding strength with the substrate materials[9]. Unfortunately, MAO-based coatings are usually consisted of one loose and porous layer with many micro-cracks and micro-pores, which accelerates the permeation of aggressive ions. Additionally, the roughness of MAO-based coatings prepared by basic electrolyte solutions should be further improved[10].

Recently, many scholars have attempted to prepare composite MAO coatings containing multifarious additives. For wear-resisting purpose, a patent duplex MAO coating combined with a graphite layer on top of it was conducted by Wang et al.[11]. The results showed that the patent duplex coatings possessed good antifriction performance. Lv et al.[12] have discovered that adding graphite grains to an electrolyte has significant effects on the microstructure of MAO coating. The results indicated that the embedded coatings were denser and less porous. Li et al. [13] have reported that Al_2O_3 particles partook in the fabrication of PEO coating with Al_2O_3 particles suspended in the aluminate electrolyte. Yang et al. [14] prepared composited MAO coating that embedded with SiC nanoparticles at different current densities. These researches revealed that additives have remarkable effects during the micro arc oxidation process, but few studies were conducted about the effect of additives on the micro-structure and wear properties of MAO coating.

Graphene, a two-dimensional carbon material and high-performance solid lubricant, possesses excellent friction and wear properties that is seldom seen in traditional materials[15-16]. Therefore, in this study, a layer of ceramic coating incorporated with graphene was prepared on Mg-Li alloy during MAO by adding graphene powders (GE) into the silicate-based electrolyte. In addition, the micro-structure, composition, tribological and corrosion behaviors of the coating incorporated with graphene were investigated and analyzed.

2. EXPERIMENTAL

2.1 MAO treatment

Mg-Li alloy specimens ($20 \times 20 \times 4$ mm) with chemical composition of 0.038% Si, 0.031% Mn, 0.028% Al, 0.011% Fe, 9% Li and 90.892% Mg, were used as substrates. Prior to the MAO treatment, these substrates were polished with SiC abrasive paper up to #2000 and then polished with Al_2O_3 paste (average size of 1 μm), to acquire a mirror surface. In addition, these specimens were also ultrasonically cleaned in ethyl alcohol for 15 min.

The electrolyte solution consisted of 10.0 g/L of sodium silicate, 5.0 g/L of sodium hydroxide, without and with addition of 0.1 g/L of GE (with an average size ranged from 0.5 μm , as provided by Beijing Carbon Century Technology Company, China) in distilled water. The pH values for the electrolytes without or with addition of GE were about 12. A homemade pulsed unipolar electrical source with power of 65 kW was utilized for micro-arc oxidation of disc specimens in a water-cooled electrolyser consisted of stainless steel, which also was used as the cathode. The temperature of the electrolytes was kept in the range 27 ~ 30 °C. The electronic power frequency was fixed at 1000 Hz. The duty ratios of pulse were equal to 40%. The whole process was carried out for 30 min under the current density of 10 A/dm².

2.2 Specimen examination

The surface morphology and the worn surface of MAO coatings were investigated by scanning electron microscope (SEM, SSX-550) equipped with energy dispersive spectrum (EDS) (for chemical

composition investigation). The phase compositions of the MAO coatings were examined by X-ray diffraction (XRD, D8 FOCUS) using Cu K α radiation, in the 2θ range of $10 \sim 90^\circ$ at a scan rate of $5^\circ/\text{min}$. Atomic force microscope (AFM, SPM9500-J3) was utilized to further investigate the surface topography and Ra of the MAO coatings. Friction and wear properties were measured utilizing a pin-on-disk machine with 3 mm diameter GCr15 balls and carried out with a load of 5 N at 200 rpm. The corrosion resistance of the substrate and MAO coatings was assessed by the potentiodynamic polarization tests using an electrochemical workstation (CS360). All experiments were conducted in a 3.5 wt% NaCl solution and the exposed area of the working electrode was 1 cm^2 . Potentiodynamic tests were performed on specimens after 1 h of immersion to achieve a stable open circuit potential (OCP), with a scanning rate of 1 mV/s from -100 mV vs. OCP to + 100 mV vs. OCP.

3. RESULTS AND DISCUSSION

3.1 Morphologies and compositions of MAO coating

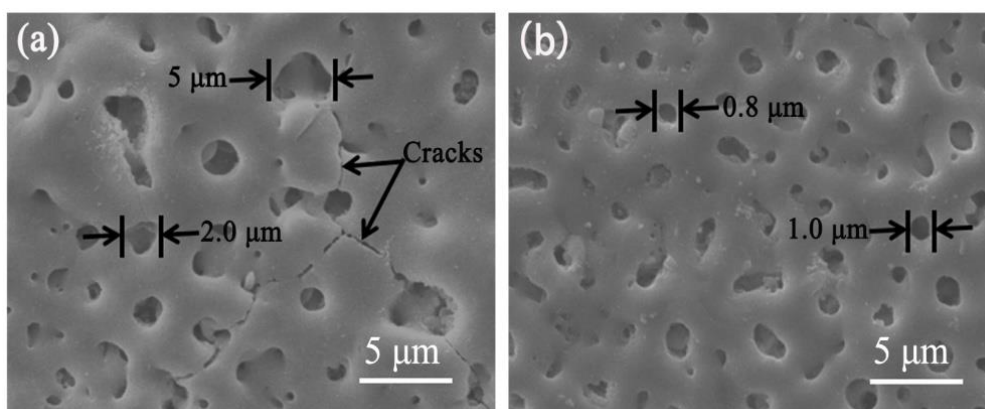


Figure 1. SEM images of: (a) MAO-based coating and (b) composite MAO coating.

Fig. 1 shows the typical SEM micro-graphs of the MAO coating formed in silicate-based electrolyte without and with GE. It can be seen that both of the MAO coatings covered by volcano-like micro-structures, which generated during discrete localized micro-discharge process. The MAO-based coating revealed several distinct micro-cracks and multiple volcanic-like micro-pores with maximum diameter of the micro-pore up to $3.5 \mu\text{m}$. As reported [17], micro-cracks were generated by the rapid solidification of the molten materials. And the micro-pores were generated by the gas bubbles which were sprayed out of the discharge channels. As shown in Fig. 1b, the size of micro-pores on the surface of composite MAO coating was significantly decreased compared with that formed without GE in silicate solution. In addition, the excessive molten oxide blocked part of the micropores and there were no distinct micro-cracks detected on the surface of the composite MAO coating. These microscopic pictures are similar to the ones for the C-containing composite coatings fabricated in previous report[10].

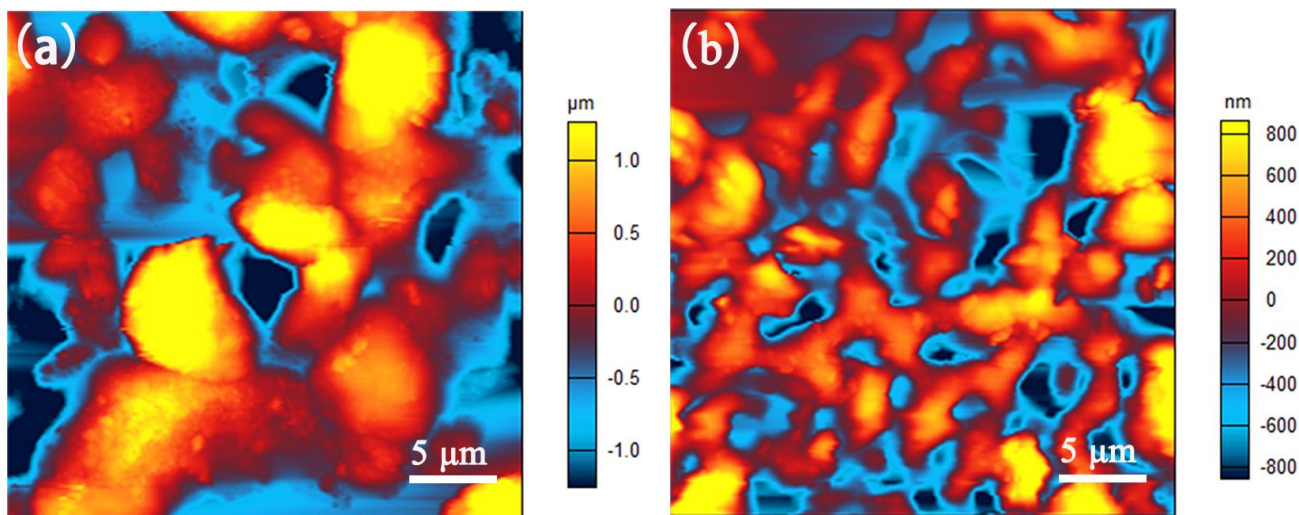


Figure 2. AFM micro-graphs of: (a) MAO-based coating, and (b) composite MAO coating.

Table 1. Examination results of the as-prepared samples.

Specimen	Rq/(nm)	Ra/(nm)	Rp/(μm)	Rz/(μm)	Skew	Area/(μm ²)
Without GE	707.90	558.60	1.95	2.08	0.12	1071.50
With GE	400.15	317.07	1.69	1.26	0.09	1049.10

To further evaluate the morphologies of the coatings prepared without and with additive of GE in the silicate-based solution, AFM was used to obtain surface roughness values of MAO coatings (Fig. 2). The results were summarized in Table 1. The average surface roughness (Ra) value of the whole 30.0 × 30.0 μm area is 558.60 nm and 317.07 nm, respectively. Obviously, the decreased surface roughness value is beneficial to reduce the friction coefficient of the MAO coatings[18].

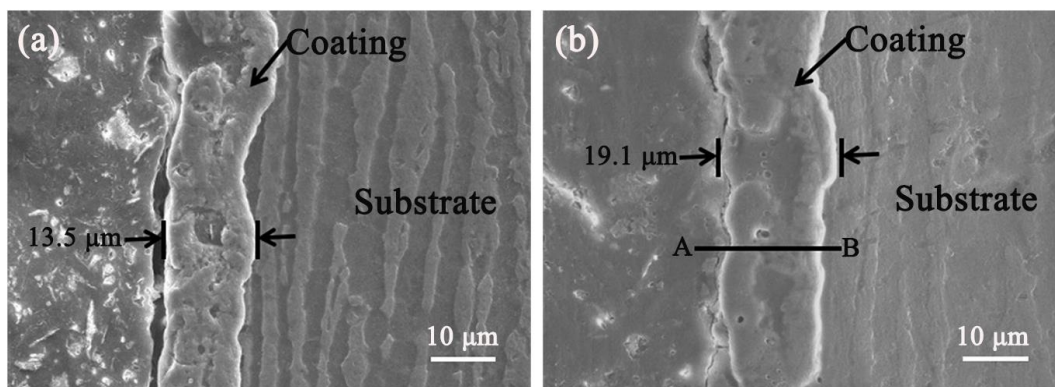


Figure 3. Cross-section SEM micro-graphs of: (a) MAO-based coating, and (b) composite MAO coating.

Cross-section morphologies of the MAO coatings are demonstrated in Fig. 3. Both of the MAO coatings occupied a bi-layered structure which is consisted of an outer porous layer and a compact inner barrier layer. This observed micro-structure was in accordance with the typical structure of MAO coatings. In addition, the thickness of the composite MAO coating was estimated to be 19.1 μm and was more compact than that formed in the absence of GE as shown in Fig. 3b. This might be attributed to the electrophoretic effect of GE. During the micro-arc discharge, some graphene were located within internal cavities, as well as the cracks, and some were wrapped in the coating surface. The synergistic effect between the two aspects improved the thickness and compactness of the coating[19].

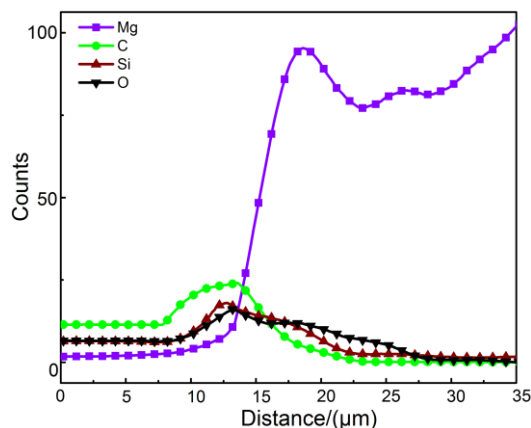


Figure 4. Cross-section elemental distribution of the composite MAO coating.

Fig. 4 displays the cross-sectional elements distribution of the composite MAO coating detected by EDS line analysis (The black line AB in Fig. 3). The concentrations of Si and O in the whole coating were relatively constant, while the concentration of C on the outer porous layer was relatively higher than that in the compact inner barrier layer of the coating. However, The presence of C in composite MAO coating suggested that dispersed graphene in the silicate-based solution participated in the discharge channels during the MAO process^[17, 19].

3.2 Phase analysis of MAO coating

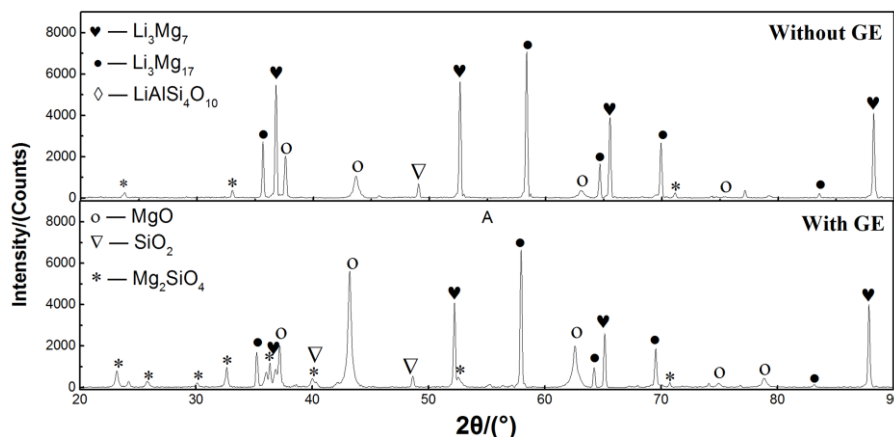


Figure 5. XRD patterns of the as-prepared samples.

Fig. 5 displays the X-ray diffraction results for both MAO coatings. As can be seen in this XRD patterns, both coatings were primarily consisted of MgO, SiO₂, and Mg₂SiO₄ phases. The intensity of Li₂Mg₇ and Li₂Mg₁₇ peaks corresponding to the substrate was strong, indicating that the MAO coatings were relatively thin and the X-ray could penetrate into the substrate. Although the element of C was detected in EDS spectrum (Fig. 4), no trace of C or carbides were detected for their lesser amount[10]. By comparing Fig. 5, it can be obviously seen that the incorporation of graphene did not transform the types of crystalline phases in the coatings formed in silicate-based solution, although they may be altered in relative amounts.

It should be realized that the total electric resistance in the electrolyte solution is the sum of the series resistances of R_w, R_e, R_a, and R_c (resistances of connections, electrolyte, anode and cathode). If we reduce the R_e value with additives to the electrolyte solution, the voltage applied on the coating will be increased spontaneously[20]. Fortunately, the addition of GE to the silicate solution improved its conductivity for adsorbing negative ions to transform into negatively charged colloidal particles. Due to the addition of GE content in the electrolyte decreased the R_e value and, the number of micro-arcs and discharging energy by a single pulse were increased remarkably. This lead to high local temperature of the micro-discharge channel and more molten oxides generated, and further resulting in an increase in the generation of hard phases and a reduction in the size of the micro-pores fabricated on the specimen surface. In fact, the suffused micro-pores by GE and embedded GE in the matrix of MAO coatings, strengthened the MAO coatings and consequently increased their surface hardnesses. In addition, dispersed GE can act as nucleation sites to promote the formation of the hard phases and prepare a finer structure[21].

When the micro-arc discharged, the silicate-based solution in the discharge channels reacted with the Mg-Li alloy substrate and formed molten oxides. At the high local temperature of the micro-discharge, vaporization of the electrolyte may concentrate, transform and sedimentate electrolyte constituents at the coating surface. The GE transported in the silicate-based solution to the coating may also be assisted by electrophoresis. Besides, within the melted region, GE may be transported by diffusion, migration and convection. However, the quantity of the molten oxides ejected from the channels was numbered and the colloidal particles continuously transferred to the anode. Thus abundance of GE could not be embedded in time and absorbed on the surface of the coating[17, 24]. Among them, there were some GE which deposited in the discharge micro-pores and micro-cracks, decreasing the diameter of the micro-pores and consequently improving density of the coating. As a consequence, adding GE to the silicate solution can cause significant changes in the surface and cross-sectional morphology as shown in Fig. 1 and Fig. 3. Therefore, the coating incorporated with GE was becoming more uniform, compact, and smooth. And the dense micro-structure is also an important factor of the increase in wear and corrosion resistance.

3.3 Tribological test

The friction coefficient evolution and wear resistance were carried out among Mg alloy substrate as well as the specimens prepared without and with GE (Fig. 6). At the start of the dry

tribological examinations of all the specimens, the friction coefficients against the counter face (GCr15 ball) gradually increased until 10 s and then decreased slightly for the remaining time. Both the increase in the friction coefficients of MAO-based coating and composite MAO coating resulted from the coarse effect of hard MgO and SiO₂ phases.

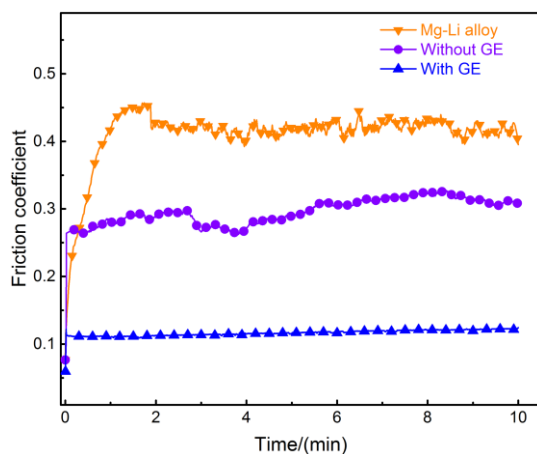


Figure 6. Friction coefficient evolution of the samples.

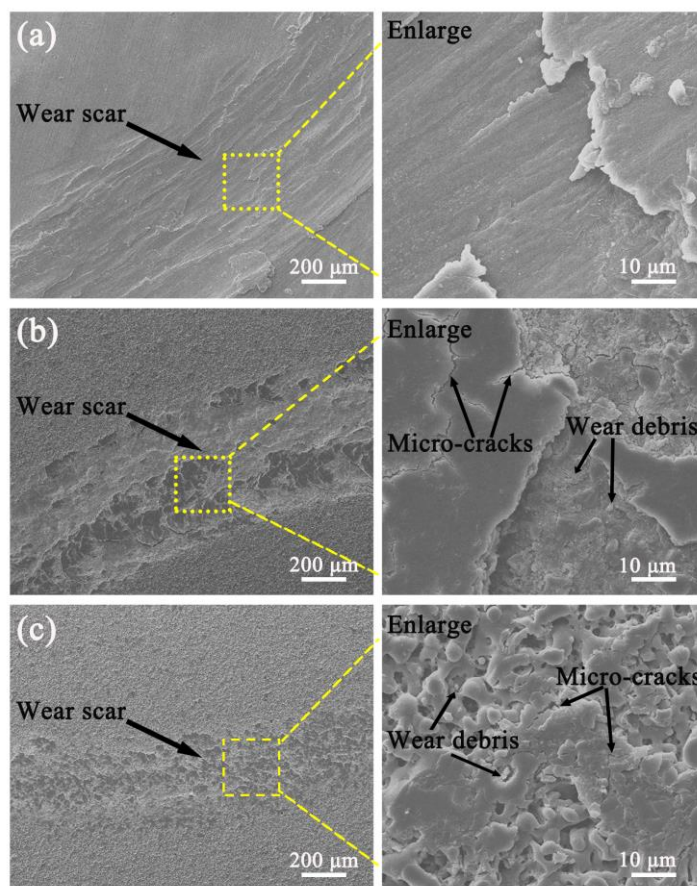


Figure 7. Worn surface morphologies of: (a) Mg-Li alloy substrate, (b) MAO-based coating, and (c) composite MAO coating.

However, a moment later, the bumps of the coatings were crushed, the newly generated debris fill the micro-pores and micro-cracks easily, the load of GCr15 ball compacts them. Therefore, the friction coefficient was reduced slightly. With the sliding continuing, the steel material transfer became increasingly striking, as a result the severe adhesive and abrasive wear mechanism possessed the sliding process which led to the high friction coefficients of Mg-Li alloy and MAO-based coating. Meanwhile, it was observed that the friction coefficient of the MAO composite coatings (0.11) was lower and stable than that of Mg-Li alloy (0.43) and MAO-based coating (0.29). Probably, the different tribological behavior between the coated specimens approved that the existence of C element and mounts of hard phases in the composite MAO coating can reduce the friction coefficient of the specimens remarkably[22].

The differences in the tribological properties were further investigated by comparing the SEM morphologies of their worn traces as their results are shown in Fig. 7. It was observed that the wear track of the composite MAO coating is much more narrow and slight than that of Mg alloy substrate and the MAO-based coating. Besides, the worn surface morphologies for the coated samples and Mg-Li alloy substrate also evidenced the complete diverse wear behavior. Fig. 7(a) shows many deep grooves and ploughs paralleling to the sliding direction caused by the deformation of Mg-Li alloy substrate. The wear track shows a typical plough zone, which indicates that the adhesive and abrasive wear are the main wear mechanism[10, 15]. From Fig. 7(b and c), the worn surface of the coatings are covered by massive micro-chipping and micro-flaking. It can be seen that the surface of MAO-based coating is nearly removed in the worn track (as shown in Fig. 7(b)). However, the wear tracks of composite MAO coating is much narrower and slighter, and the worn surfaces appear relatively smooth.

The wear resistance of the specimens is principally connected with their friction coefficient and surface hardness. The synergistic effects of the decrease of friction coefficient and increase of surface hardness are the leading cause for improvement in tribological performance[10,11,20]. Initially, graphene by filling the micro-pores and micro-cracks of the composite MAO coating reduce its roughness and friction coefficient, densify the coating and increase its thickness. Additionally, dispersed graphene in the matrix of composite coatings occupy a pinning and second phase strengthening role which improve the hardness of the composite coating. As a result, the synergistic effects of reduction in friction coefficient and enhancement in surface hardness of the composite MAO coating diminish the ploughing effect which induces reduction in the depth of wear track.

3.4 Potentiodynamic polarization test

It was well known that the corrosion resistance of the coated specimens was affected by several essential elements such as composition, thickness and compactness of the porous layer. The corrosion resistances of Mg-Li alloy substrate and MAO coatings were measured by potentiodynamic polarization tests in the 3.5 wt% NaCl solution and the polarization curves for different specimen were presented in Fig. 8. Corrosion potential (E_{corr}), corrosion current density (i_{corr}), annual corrosion rate (i_a) and the anodic/cathodic Tafel constants (β_a , β_b) were derived directly from the polarization curves

by Tafel region extrapolation. The polarization resistance (R_p) can be acquired from Stern-Geary equation[23]:

$$R_p = \frac{\beta_a \times \beta_b}{2.3 \times I_{corr} \times (\beta_a + \beta_b)}$$

All the parameters values were summarized in Table 2.

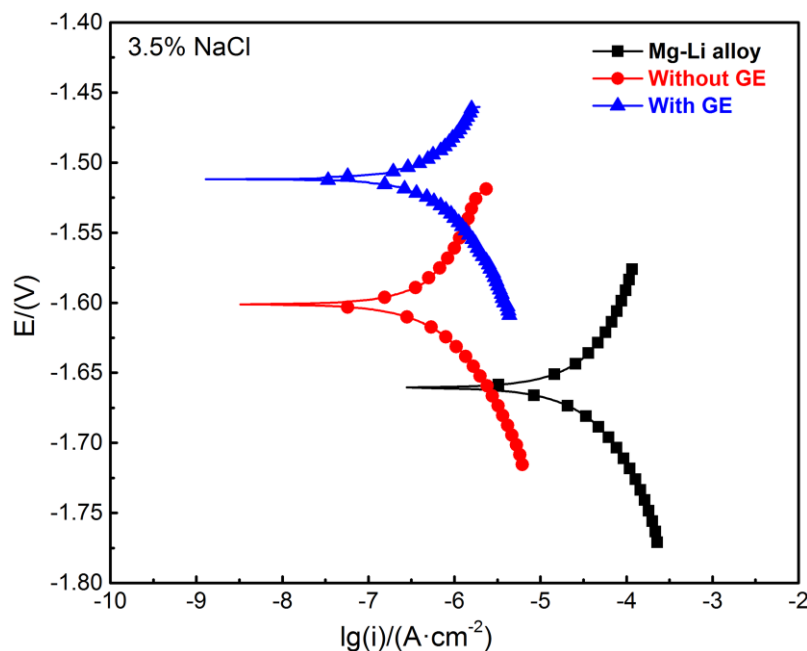


Figure 8. Polarization curves of the as-prepared samples.

Table 2. Electrochemical parameters from polarization curves.

Specimens	$\beta_a/(V/dec)$	$\beta_b/(V/dec)$	$I_{corr}/(A \cdot cm^{-2})$	$E_{corr}/(V)$	$R_p/(\Omega)$	$I_a/(mm/a)$
substrate	0.37	0.22	9.21×10^{-5}	-1.66	6.44×10^2	2.4
Without GE	0.27	0.14	1.20×10^{-6}	-1.60	4.83×10^4	1.2×10^{-2}
With GE	0.034	0.059	1.06×10^{-7}	-1.512	8.90×10^4	1.1×10^{-3}

By combination Fig. 8 and Table 2, it obviously showed that the corrosion resistance of both specimens with MAO coating are improved significantly compared with the Mg-Li alloy substrate. For the MAO-based coating, its corrosion potential has little shift to the positive direction (59 mV) which is nearly close to the E_{corr} of the Mg-Li alloy substrate. This case may be contributed to the corrosive ions (Cl^-) penetration through the micro-pores and micro-cracks of the porous layer. Furthermore, the corrosion current density decreased from $9.21 \times 10^{-5} A/cm^2$ to $1.20 \times 10^{-6} A/cm^2$, almost by two orders and the polarization resistance increased significantly from $6.44 \times 10^2 \Omega$ to $4.83 \times 10^4 \Omega$. And what's

more, the shift of corrosion potential to positive direction of the composite MAO coating is significant (148 mV) and its corrosion current density (1.06×10^{-7} A/cm²) decreased by more than three orders of the magnitude compare with that of Mg-Li alloy substrate. In addition, the polarization resistance of the composite coating was estimated at up to $8.91 \times 10^4 \Omega$ which is approximately 138 times the value of R_p for the Mg-Li alloy substrate. All these indicate that the composite MAO coating possesses the excellent corrosion resistance. This can be interpreted by the SEM MORphologies in Fig. 1 b, which shows that the pores size in composite coating reduces remarkably[24].

It is obvious that two major essential elements can cause the composite MAO coating to exhibit lower corrosion rate than MAO-based coating. The mainly factor is thickness of the MAO coating. Composite MAO coating displayed much thicker ceramic coating which could effectively postpone the penetration or diffusion of aggressive ions, and hence prevent corrosion of Mg-Li alloy when exposed to the corrosive liquid. Compactness and uniformity of the composite MAO coating is another factor that influenced the corrosion rate of the specimens. It is well known that the porous layer possesses an porous structure which allowed penetration of aggressive ions to the Mg-Li alloy substrate and accelerated corrosion to proceed. Therefore, the composite MAO coating with a more uniform and serried layer before immersion served as a protective layer to prohibit further corrosion attack[13,17]. The enhanced corrosion resistance of the composite MAO coating can be attributed to the more compact structure and thickness which acted as a barrier against infiltration of aggressive ions (Cl⁻) from corrosive liquid into the coating.

4. CONCLUSION

In this paper, ceramic coatings were prepared on Mg-Li alloy by using micro-arc oxidation in silicate solution without and with the addition of GE. The GE-added MAO composite coating showed more uniform and compact with less structural defects compared with the MAO-based coating. XRD analyses proved that the incorporation of graphene into the MAO coatings altered the relative amounts of hard MgO and SiO₂ phases. Both the average surface roughness value and friction coefficient of the composite coating decreased significantly after adding GE into the electrolyte. The wear track of the composite coating was much more narrow and slight than that of Mg-Li alloy substrate. Highest R_p and lowest I_{CORR} values were obtained after the application of the composite coatings. The results demonstrated that the incorporation of graphene into the coatings can improve the wear and corrosion resistance of the Mg-Li alloy remarkably.

ACKNOWLEDGEMENT

This work was supported by the National Natural Science Foundation of China (Grant No.51601015).

References

1. F. Feng, S. Y. Huang, Z. H. Meng, J. H. Hu, Y. Lei, M.C. Zhou and Z. Z. Yang, *Materials Science & Engineering A*, 594 (2014) 334.

2. S. Y. Wang, Y. P. Xia, L. Liu and N. C. Si, *Ceramics International*, 40 (2014) 93.
3. H. X. Liu, Q. Xu, Y. H. Jiang, C. Q. Wang and X. W. Zhang, *Surface & Coatings Technology*, 228 (2013) S538.
4. F. Chen, H. Zhou, B. Yao, Z. Qin and Q. F. Zhang, *Surface & Coatings Technology*, 201 (2007) 4905.
5. M. Daroonparvar, M.A.M. Yajid, H.R. Bakhsheshi-Rad, N.M. Yusof, S. Izman, E. Hamzah and M.R. Abdul Kadir, *Vacuum*, 108 (2014) 61.
6. H. R. Bakhsheshi-Rad, E. Hamzah, M. Daroonparvar, M. A. M. Yajid and M. Medraj, *Surface & Coatings Technology*, 258 (2014) 1090.
7. H. H. Elsentriecy, J. Qu, H. M. Luo, H. M. Meyer, C. Ma and M. F. Chi, *Thin Solid Films*, 568 (2014) 44.
8. T.M. Yue, H. Xie, X. Lin, H.O. Yang and G.H. Meng, *Journal of Alloys & Compounds*, 587 (2014) 588.
9. J. H. Jiang, Qi. Zhou, J. S. Yu, A. B. Ma, D. Song, F. M. Lu, L. Y. Zhang, D. H. Yang and J. Q. Chen, *Surface & Coatings Technology*, 216 (2013) 259.
10. Y. L. Hua, Z. G. Zhang and W. Li, *Surface & Coatings Technology*, 291 (2016) 70.
11. Y.M. Wang, B.L. Jiang, T.Q. Lei and L.X. Guo. *Applied Surface Science*, 246 (2005) 214.
12. G. H. Lv, H. Chen, W. C. Gu, W. R. Feng, L. Li, E. W. Niu, X. H. Zhang and S. Z. Yang. *Current Applied Physics*, 9 (2009) 324.
13. X. J. Li and B. L. Luan, *Materials Letters*, 86 (2012) 88.
14. Y. Yang and Y. H. Liu, *Journal of Materials Science & Technology*, 26 (2010) 1016.
15. D. Berman, A. Erdemir and A. V. Sumant, *Materials Today*, 17 (2014) 31.
16. H. Q. Li, Y. T. Xie, K. L., L. P. Huang, S. S. Huang, B. Z. Zhao and X. B. Zheng, *Ceramics International*, 40 (2014) 12821.
17. J.H. Gao, S.K. Guan, J. Chen, L.G. Wang, S.J. Zhu, J.H. Hu and Z.W. Ren, *Applied Surface Science*, 257 (2011) 2231.
18. S. Abbasi, F. G. Fard, H.R. Rezaie and S.M.M. Mirhosseini, *Applied Surface Science*, 261(2012) 37.
19. S. Y. Wang, N. C. SI, Y. P. Xia and L. Liu. *Transactions of Nonferrous Metals Society of China*, 25 (2015) 1926.
20. H. Niazi, S. Yari, F. G. Fard, M. Shahmiri, W. Wang, A. Alfantazi and R. Bayati. *Applied Surface Science*, 353 (2015) 1242.
21. H. X. Li, R. G. Song and Z. G. Ji, *Transactions of Nonferrous Metals Society of China*, 23 (2013) 406.
22. K. J. Ma, M. M. S. Al Bosta and W. T. Wu, *Surface & Coatings Technology*, 259 (2014) 318.
23. K. M. Lee, K. R. Shin, S. Namgung, B. Yoo and D. H. Shin, *Surface & Coatings Technology*, 205 (2011) 3779.
24. G. H. Lv, H. Chen, W. C. Gu, W. R. Feng, L. Li, E. W. Niu, X. H. Zhang and S. Z. Yang, *Current Applied Physics*, 9 (2009) 324.